GA-A14045
UC-77

MECHANICAL ASPECTS OF THE THERMAL SHIELDING FOR THE GAS-COOLED FAST BREEDER REACTOR

by
L. E. Penzes, S. K. Bhat, and
V. Jovanovic

Prepared Under
Contract E(04-3)-167
Project Agreement No. 23
for the
San Francisco Operations Office
U.S. Energy Research and Development Administration

General Atomic Project 3228 Date Published: October 18, 1976

CEB

ABSTRACT

Heat transfer, hydrodynamics, and structural analysis methods relevant to the gas-cooled fast breeder reactor (GCFR) shielding design are reviewed and evaluated, and results of heat transfer and hydrodynamic analyses are presented. Owing to uncertainties in pressure loss correlations and the complexity of the flow field upstream of and around the upper axial shield assembly, a flow test for this region is recommended to verify analytical pressure loss calculations. Results of heat transfer and hydrodynamic analyses for the 300-MW(e) GCFR reference shielding design are discussed. Preliminary heat transfer analyses indicate that the inner radial shield design should be changed to provide adequate cooling. By providing an additional coolant passage in the inner radial shield, the predicted shield temperatures were reduced to acceptable levels. Current technical literature on structural methods is also reviewed, and fracture mechanics methods are described. Structural analysis methods discussed in this report include simplified stress analysis and stress analysis based on fracture mechanics. Stress analysis of the shield assemblies will be preceded by simplified stress analysis which will be used to size some of the structural components of the shield assembly. Fracture mechanics analysis is required for the final calculations.

1. INTRODUCTION

This report discusses the mechanical design of the radiation shielding in the gas-cooled fast breeder reactor (GCFR). The objective of the design program is to provide radiation shielding which, in addition to supplying adequate attentuation to damaging radiation, withstands the effects of the environment for the requisite 30 yr without maintenance. The problem of proving that the design finally selected will meet this objective is examined. For normal operation, the environmental conditions considered to have the greatest effect on the design include (1) core outlet helium temperatures of 550°C (1022°F), (2) total neutron fluences of 1.0×10^{23} cm^{-2}, (3) a pressure of 9 MPa (1305 psia), and (4) for emergency and faulted conditions, seismic excitation and pressure blowdowns. The actual number and severity of these conditions has not yet been established, but the methods of proving the design are expected to be independent of these factors.

Determination of the following variables, which are considered to be the most important, are discussed: (1) the effect of the shielding on the helium flow and the characteristics of the flow necessary to establish heat transfer coefficients between the helium and the shielding material; (2) temperature distributions through the shielding thickness; and (3) methods to assess the ways in which structural materials are affected by temperature distribution, pressure, flow-induced vibration, static weight, seismic forces, irradiation-induced swelling enhancement of thermal creep effects, and embrittlement.

2. HEAT TRANSFER AND HYDRODYNAMICS

The shielding structures must be designed to provide minimum resistance to coolant flow. Furthermore, the coolant flow rates around all shielding structures must be sufficient to remove the heat deposited in the structures by neutrons and gamma rays. The adequacy of the coolant flow rates is determined based on the temperatures in the shield materials and the impact of the operating environment on the structural and material integrity of the shield. Furthermore, the adequacy of the analytical tools and methods used in the coolant flow and shield temperature predictions must be established.

2.1. ANALYTICAL METHODS

The purpose of this effort was to define and evaluate the analytical tools and methods for determining (1) flow distribution and pressure loss related to coolant flow in and around the shielding structures and (2) temperature distributions in the shielding structures.

2.1.1. Coolant Flow Prediction Methods

Several fluid flow network analysis computer codes are available at General Atomic (GA) which can be used to predict the coolant flow characteristics in and around the shielding structures under steady-state conditions. Two of these codes, FLAC (Refs. 1, 2) and SPIFFS (Ref. 3) are particularly suitable for these analyses. Both codes can solve large or small, arbitrarily connected, generalized fluid flow networks. The original version of the SPIFFS code, as obtained from Shell Oil Company, has the capability to simulate steady-state, single-phase, isothermal, incompressible and compressible fluid flow in smooth and/or rough conduits of circular cross section. It permits the simulation of "lumped pressure

change" in-line devices such as pumps, compressors, and check valves and can be applied to the design of new networks or additions to existing networks. SPIFFS also has a provision for pressures and/or flow rates to be individually specified at any number of arbitrary locations, and it performs many diagnostic checks to ensure the feasibility of the modeled network. The SPIFFS code has been modified at GA to accommodate noncircular geometry and dynamic loss coefficients. It is currently being modified to accommodate nonisothermal flow problems.

The main solution scheme is different in the two programs: FLAC uses the successive substitution method, and SPIFFS uses a direct matrix manipulation method. The method of successive substitution works best when all branch conductances are of the same order of magnitude. However, when a branch conductance is much higher than the mean conductance value, convergence problems are usually encountered. This type of convergence problem does not arise in the SPIFFS solution algorithm. In order to efficiently accommodate large flow networks, the SPIFFS solution algorithm utilizes the technique of decomposition of narrow band width, positive-definite, nonsingular symmetric matrices; this technique has been successfully applied to solution of rigid-body equation systems in stress analysis codes. The SPIFFS code also utilizes an efficient, dynamic storage allocation method, thus taking maximum advantage of the space available for storage of the data and the solution matrix. Although the SPIFFS code is preferable because of its better converging solution algorithm, the SPIFFS and FLAC codes have adequate capabilities for steady-state fluid flow analysis around the shielding structures. In fact, virtually identical results for one test case were obtained with the two codes (Ref. 4).

The resistances in fluid flow networks can be calculated from the pressure loss coefficients available in the literature. The pressure loss coefficients account for frictional and local losses such as those due to changes in flow direction, cross-sectional area, shape along the flow path, or various obstructions to the flow. These loss coefficients were

mainly obtained from experimental data, although some were theoretically derived. Reference 5 contains a good collection of pressure loss coefficients for various configurations.

A study was recently conducted at GA to review the latest available data on the thermodynamic and transport properties of helium as applied to gas-cooled reactor design (Ref. 6). This study indicated that there are only very minor differences in the thermodynamic data determined from the various calculational formulas in the pressure and temperature ranges of interest. Examination of transport property data revealed larger differences between investigations; therefore, new correlations were developed for thermal conductivity and viscosity from experimental data.

The applicability and validity of the original version of the SPIFFS code has been demonstrated (Ref. 4) using the formal verification procedure (Ref. 7); new versions will also be verified. Although the FLAC code has not undergone the formal verification procedure, it does meet one criterion sufficient for verification; i.e., it is a recognized computer code in the public domain which has had enough use to justify its applicability and validity without further demonstration.

Even though the computer codes have been verified, the validity of the analytical methods must also be established. Various uncertainties in the analytical methods have been evaluated, and the uncertainties in the helium thermodynamic and transport properties have been determined (Ref. 6). For GCFR pressure and temperature ranges, the error bounds for thermodynamic properties have been specified to be less than 0.5%; for thermal conductivity and viscosity correlations, the standard deviations have been calculated to be 2.4% and 1.5%, respectively. Uncertainties associated with the primary coolant pressure drop calculations were evaluated for the 300-MW(e) reference design, as discussed in Section 2.2.1. Available experimental correlations for some local pressure loss coefficients are considered to be inaccurate and unreliable, and experimental verification

of pressure loss characteristics for such configurations is recommended. One such case is the flow upstream of and around the upper axial shield assembly from the cold duct exit to the grid plate, as shown in Fig. 1. This flow is characterized by the expansion from the cold duct into the upper plenum, the flow past core assembly extension members through the upper plenum (not shown in Fig. 1), a 90-deg turn combined with mixing of streams from the three cold ducts, and the flow past the upper axial shield assembly. Owing to the complexity of the flow field and the lack of reliable pressure loss correlations for these configurations, it is recommended that a flow test be conducted for this region to verify the analytical pressure loss calculations.

2.1.2. Heat Transfer Methods

Temperature profiles in the shielding structures will be calculated by using one-dimensional and/or multidimensional heat transfer techniques and applying internal heat generation rates obtained from physics analyses and convective heat transfer coefficients determined from coolant flow predictions. Several heat transfer computer codes are available which can be used to perform these analyses. The TAC2D code (Ref. 8) will be used mainly because of the simplicity of input. This code (version TFMABC 75-1) was verified (Ref. 9) using the formal verification procedure. Other more versatile codes such as SINDA (Ref. 10) are also available.

2.2. ANALYSES AND RESULTS

The hydrodynamic and heat transfer analyses performed in order to predict coolant flow characteristics around the shielding structures and calculate the temperature distributions in the shielding structures are based on the 300-MW(e) GCFR reference prestressed concrete reactor vessel (PCRV) design configuration and primary coolant flow parameters given in Ref. 11. Additional shielding heat transfer and hydrodynamic analyses are being performed for alternate shielding configurations and low primary system pressure loss configurations. [Studies are currently in progress

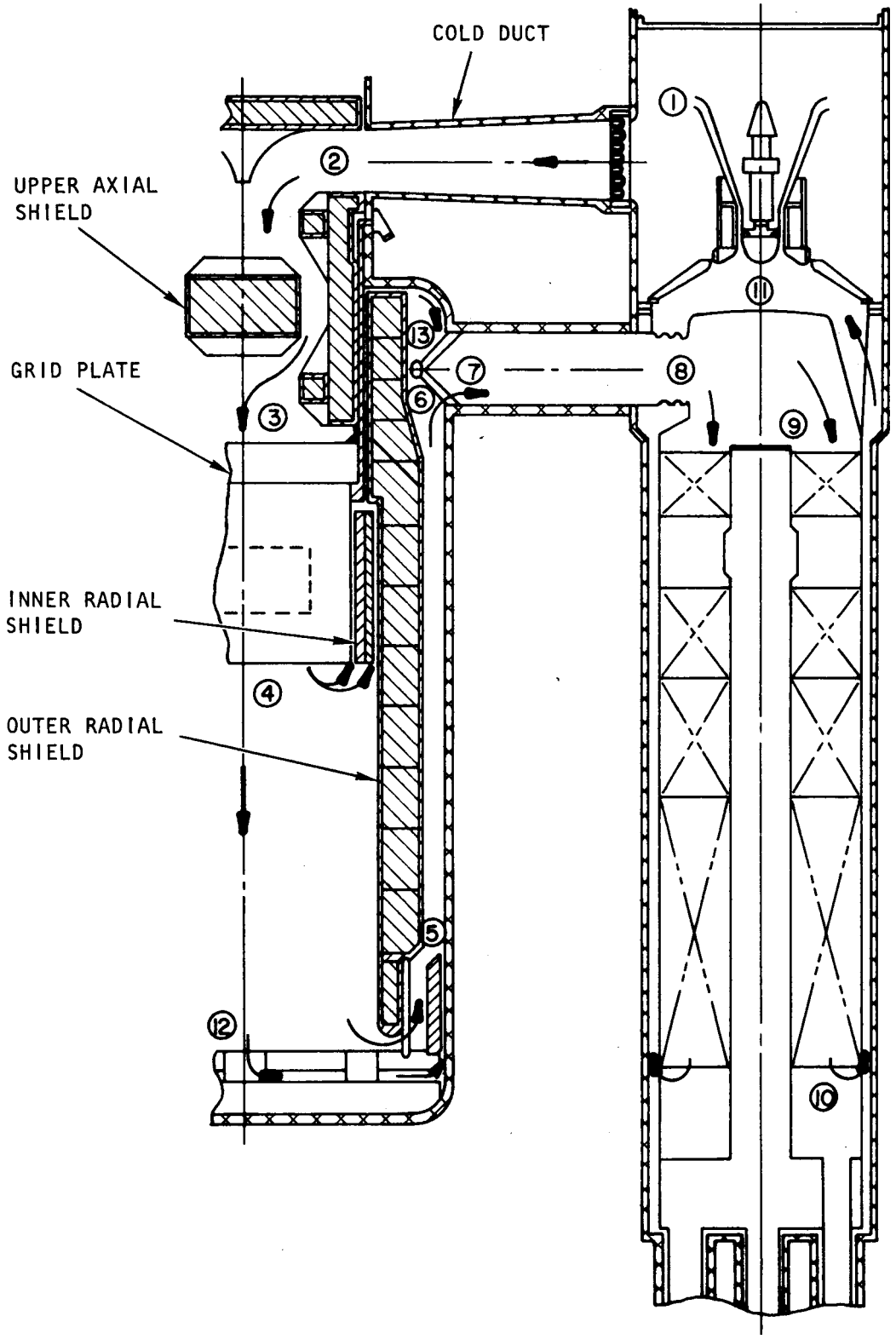

Fig. 1. Helium flow path and pressure locations

to assess the feasibility of reducing the primary system pressure loss from the reference design value of 372.4 kPa (54 psi) to 275.8 kPa (40 psi)]. Some of the alternate shielding configurations being analyzed include a new upper axial shielding configuration and a revised lower axial shielding configuration. The results of these analyses will be presented in a final report.

2.2.1. Coolant Flow Characteristics

Hydrodynamic analysis of the primary coolant system, including the flow around the shielding structures, was performed in which reference PCRV configuration and coolant flow parameters (Ref. 11) were assumed; the main and parallel flow paths through a single loop of the primary system are shown in Fig. 1. The following four networks were considered:

1. Network 1, which comprises only the main flow path (points 1 to 11).

2. Network 2, which comprises the main flow path (points 1 to 11), and two parallel flow paths (points 4 to 13 and 12 to 5).

3. Network 3, which comprises the flow paths described in network 2 plus the coolant cross flow through 1.27-cm (0.5-in.) wide passages between the segments of the outer radial shield.

4. Network 4, which comprises the flow paths described in network 2 plus the coolant cross flow through 2.54-cm (1.0-in.) wide passages between the segments of the outer radial shield.

Coolant flow passages in these networks were characterized, and an analytical flow network model was devised. Existing pressure loss correlations, taken mainly from Ref. 5, were employed to calculate the pressure loss in each of the flow paths. Numerical values yielding the most conservative

results were used because of the uncertainties associated with some friction factors and loss coefficients for change in direction, cross-sectional flow area (i.e., sudden expansion or contraction), shape, and other types of losses. The flow network analysis computer code FLAC (Ref. 2) was used to predict coolant flow and pressure drop characteristics for the four flow networks. The results of these analyses are reported in Section 8.1.4 of Ref. 12 and Section 13.2.2.1 of Ref. 13.

Subsequent to this analysis, uncertainties associated with the calculated primary coolant pressure drops in ducts and reactor plenums and in and around shielding structures were evaluated. In determining the uncertainties in pressure drop calculations, two significant contributing factors were considered: manufacturing variablity and analytical modeling uncertainties. The uncertainty band was calculated about the expected pressure drop value; these results and the rationales and assumptions made in calculating the uncertainties are presented in Table 1. The limits of the uncertainty band represent the extremes of the expected pressure drop under normal operating conditions. This study indicates that in the normal operating range, the dependent variable, i.e., pressure drop, is nonlinearly dependent on the independent variables, i.e., radius ratio, bend angle, etc., which are implicit functions of pressure drop. Therefore, the variability of pressure drop about the expected value is skewed.

2.2.2. Shield Heating and Cooling

Steady-state heat transfer analyses of the radial shielding structures have been performed for normal operating conditions at full power to calculate the temperature distributions in the inner and outer radial shielding structures and assess the cooling requirements for the structures. The energy deposition rates in the shield were obtained from physics analyses, and the convective heat transfer coefficients for shielding boundaries were calculated based on the coolant flow characteristics predicted in the hydrodynamic analysis (Section 2.2.1). An analytical thermal

TABLE 1
PRIMARY COOLANT PRESSURE DROPS IN DUCTS AND PLENUMS AND ASSOCIATED UNCERTAINTY BANDS FOR NORMAL OPERATING CONDITIONS (AT 100% POWER)

Location	Pressure Drop Expected	Uncertainty Band (% of Expected)	Rationale
Diffuser outlet to shield inlet (points 1 to 2)	1.37	±8	±8% is allowed for uncertainties associated with loss coefficients for change in flow cross-sectional area, i.e., expansion in the circulator plenum followed by contraction in the cold gas cross duct. (Uncertainties in loss coefficients may result from manufacturing variability and/or calculational modeling uncertainties. This also applies to other locations listed below.)
Shield inlet to grid plate (points 2 to 3)	3.81	+19.7, -16.5	+19.7% and -16.5% uncertainty bands result from uncertainties associated with loss coefficients for (1) change in flow direction, (2) change in flow cross-sectional area, and (3) flow past obstructions, i.e., assembly lock extension members through upper plenum. Note that the variance of pressure drop about the expected value is skewed owing to nonlinear behavior of loss coefficients with respect to independent variables, e.g., radius ratio, aspect ratio, bend angle, etc.
Core exit to radial shield turn (points 4 to 5)	0.48	+31, -13	+31% and -13% uncertainty bands result from uncertainties associated with loss coefficients for (1) change in flow direction (two 90-deg and two 45°-deg bends) and (2) change in flow cross-sectional area (sudden expansion and contraction).

TABLE 1 (Continued)

Location	Pressure Drop Expected	Uncertainty Band (% of Expected)	Rationale
Radial shield (points 5 to 6)	0.05	∿0	
Turn from radial shield to hot gas cross duct (points 6 to 7)	0.52	+21, -12.4	+21% and -12.4% uncertainty bands result from uncertainties associated with loss coefficients for (1) change in flow direction (90-deg bend with turning vanes) and (2) change in flow cross-sectional area (sudden contraction).
Hot gas cross duct (points 7 to 8)	0.05	∿0	

model of the radial shields at the core midplane was constructed. The model consisted of stainless steel and graphite material blocks, helium coolant blocks, and helium gaps; the helium in the gaps was assumed to be stagnant. Variations in material properties with respect to temperature were taken into account, and the two-dimensional heat transfer computer code TAC2D (Ref. 8) was employed for the analysis.

The analysis was first performed for the radial shield design and energy deposition rates corresponding to the three-row blanket configuration. The radial shield geometry used in the analysis is shown in Fig. 13.7 of Ref. 13, and the energy deposition rates used are shown in Fig. 13.3 of Ref. 14. The effects on temperature distributions of different graphite thermal conductivities (irradiated and unirradiated), energy deposition rates, and gap sizes at material interfaces were examined. The predicted temperature distribution for one typical case [assuming irradiated graphite and 0.63-cm (0.25-in.) wide helium gaps] is shown in Fig. 13.8 of Ref. 13. The maximum temperature of 910°C (1670°F) was predicted to occur in the graphite section of the inner radial shield. In all cases considered, temperatures in the supporting steel section of the inner radial shield were near or exceeded the carburization temperature of 816°C (1500°F) for 304 stainless steel. These high temperatures indicate that the inner radial shield should be redesigned to provide adequate cooling. The effect of energy deposition rates on temperature distribution was also studied using one-half and one-third the rates obtained from the physics analyses. The results, which are presented in Fig. 13.9 of Ref. 13, indicate that this effect is significant. The analysis was also performed for a modified radial shield configuration having boronated graphite in the outer shield, as shown in Fig. 13.4 of Ref. 12. High temperatures and temperature gradients were again predicted, as shown in Fig. 13.6 of Ref. 12. A maximum temperature of 917°C (1683°F) was predicted for the graphite section of the inner radial shield.

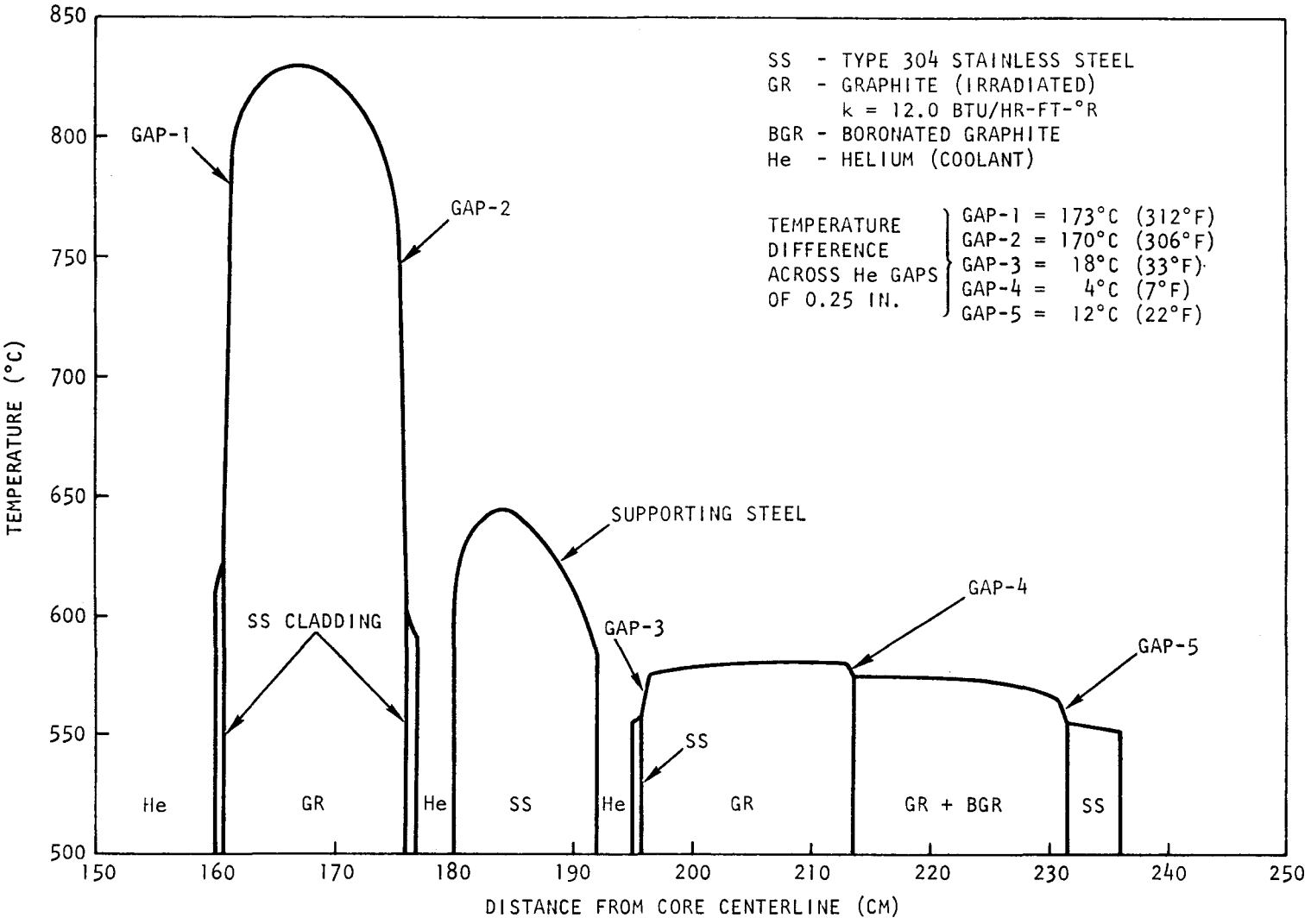

Fig. 2. Temperature distribution in the GCFR radial shield at the core midplane for configuration 1 with four coolant passages

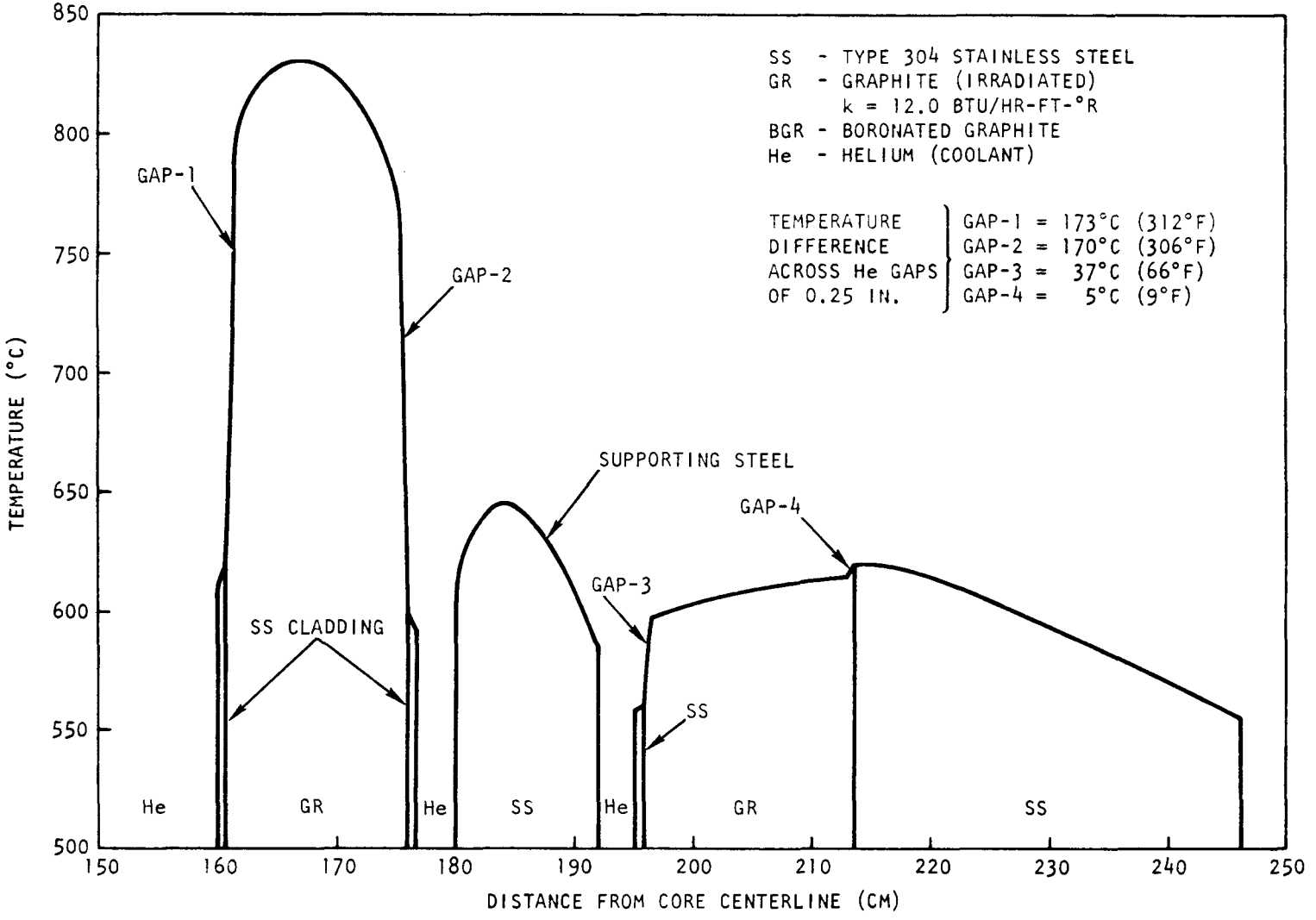

Fig. 3. Temperature distribution in the GCFR radial shield at the core midplane for configuration 2 with four coolant passages

In order to reduce the high temperatures and temperature gradients in the inner radial shield, the graphite section of the shield (including the cladding) was assumed to be separated from the supporting steel section, and an additional coolant passage was introduced, as illustrated in Fig. 13.5 of Ref. 12. The resulting temperature distribution is shown in Fig. 13.7 of Ref. 12. With the addition of a coolant passage, the maximum temperature in the graphite section of the inner radial shield was reduced to 768°C (1415°F), and that in the supporting steel section of the inner radial shield was reduced to 622°C (1152°F). Thus, provision of an additional coolant passage between the graphite and steel sections of the inner radial shield resulted in temperatures which were within the physical limitations imposed on shielding materials.

The analysis was also performed for the revised energy deposition rates corresponding to the two-row blanket design (Ref. 15, Section 10.5.3). The proposed shield configurations and the temperature profiles corresponding to these configurations are shown in Figs. 2 and 3. An additional coolant channel between the graphite and supporting steel sections of the inner radial shield was again assumed for more effective heat removal. For configurations 1 and 2, the maximum predicted temperature in the graphite region of the inner radial shield was 832°C (1529°F), which was approximately 64°C (114°F) higher than the corresponding temperature for the three-row blanket design. The surface temperatures of the inner radial shield graphite ranged from 771°C (1420°F) to 795°C (1463°F). These temperatures were approximately 44°C (1420°F) to 54°C (98°F) higher than the corresponding temperatures for the three-row blanket design. The maximum predicted temperature in the supporting steel section of the inner radial shield was 646°C (1195°F), which was 24°C (43°F) higher than the corresponding temperature for the three-row blanket design. The results of this analysis indicate that the temperature profiles in the radial shield for the two-row blanket design are higher than those for the three-row blanket design primarily because of approximately 50% and 20% increases in the energy deposition rates in the inner and outer radial shields, respectively,

for the two-row blanket design. The increase in the energy deposition rates can be attributed to a reduction in the neutron attentuation associated with the removal of the third row of blanket assemblies. Although the temperatures for the two-row blanket design were higher than those for the three-row blanket design, they were within the range found satisfactory in other reactor applications of these materials.

3. STRUCTURAL ANALYSIS ASSESSMENT

This section discusses current techniques for evaluating the stresses and strain determined for the shield structures. A review of the current technical literature on the subject is also presented.

3.1. REVIEW OF CURRENT PUBLICATIONS

Current fast breeder program publications have been reviewed. Reference 16 examines the combined effects of high temperatures [as high as 760°C (1400°F)] and long-term fluences (in some cases as high as 10^{23} n/cm^2) on various candidate steel materials, i.e., 304, 316, and 321 stainless steel. Reference 16 illustrates the combined effects of creep and irradiation-induced swelling; however the maximum recorded fluences of these tests are less than half of GA's requirements. An excellent review of shielding materials is given in Ref. 17, which investigates the material properties of various graphites and boronated graphite and the applicability of different steel alloys (304, 316, 430 stainless steel, etc.) to cladding. The structural behavior of these alloys is also examined. Of all the recent technical papers studied, Ref. 18 appears to be useful and the most applicable to the problems encountered. Unfortunately, Ref. 18 is very brief. The Clinch River breeder reactor preliminary safety analysis report (Ref. 19) is the most detailed effort in this field. This report covers the safety aspects and design criteria of the shield, but does not supply solid background information relating to these criteria. Without more information about steady and transient loads, temperatures, fluence levels, and consequent stresses and allowable values, the design criteria for the Clinch River breeder reactor may not be directly applied to the GCFR shield design. The design criteria of Ref. 19 seem to be based upon tentative design practice which is probably conservative rather

than on a detailed analysis considering a brittle failure mode. Regarding the removable radial shield, Ref. 19 states, "the removable radial shielding is in a preliminary phase of design; thus, stress analysis taking into account the effects of environmental conditions has not yet been completed. Analysis will be conducted on the following considerations: thermal stresses and strains, refueling and handling stresses, strain limits for brittle material, and effects of irradiation-induced swelling and creep on the core restraint system."

Reference 20 provides useful information on material properties, but the scope of this book is not sufficient. Reference 21 is a basic reference for high-temperature analysis of pressure vessels, however this code case does not consider the effect of irradiation. Of the available textbooks reviewed, Refs. 22 and 23 represent the classical knowledge in creep theory; Ref. 24 covers state-of-the-art information and techniques, considering high-temperature and long-term effects, and Ref. 25 presents an excellent review of the interaction between thermal stress, creep, and low-cycle fatigue.

A comprehensive report (Ref. 26) was recently published which examines the current state-of-the-art design criteria supplementing the code case, including the effects of irradiation on high-temperature-induced creep, fatigue, and strain limits as well as fracture mechanics considerations. This report recommends the following criteria:

1. Below a fluence limit of 10^{20} n/cm^2 ($E > 0.1$ MeV), the effect of irradiation can be ignored for 304 and 316 stainless steel.

2. Above the fluence limits of Table 5.1 of Ref. 26, the effect of irradiation may be accounted for by modifying the rules of Code Case 1592 according to the requirements of Ref. 26.

3. For irradiated materials, the method of fractural mechanics should be used to evaluate the structures for brittle failure.

The fracture mechanics technique is strongly established and widely used in the aerospace industry for low-cycle fatigue analysis of jet engine disks, stress analysis of B-1 components, etc. It is even used in commercial power plant designs, e.g., in Combustion Engineering's fossil-fuel-fired steam generator.

An excellent short review of fracture mechanics is given in Ref. 27. Reference 28 is one of the best textbooks on fracture mechanics, and Ref. 29 presents useful and valuable information on the fractural properties of 304, 316 etc., stainless steel.

3.2. METHODS OF STRUCTURAL ANALYSIS

Stress analysis of the shield assemblies will be preceeded by simplified stress analysis. The simplified stress analysis will be used to size the structural components of the shield assembly. In addition to a final analysis, a fracture mechanics analysis, described below, is required.

3.2.1. Simplified Stress Analysis

Simplified methods will be applied to analyze the different radial shield configurations assuming steady-state loads. The corresponding thermal stresses, thermal expansions, creep, and relaxations will be calculated. The acceptability of the stresses and strains obtained will be determined using ASME Code Case 1592 as modified and supplemented by Ref. 26.

3.2.2. Structural Analysis Based on Fracture Mechanics

Structural analysis of materials having low ductility owing to high temperature and fluence must include analysis by fracture mechanics. This is the state-of-the-art technique for analysis of brittle materials with low residual ductility.

Conventional design theories account for stress, material strength, and stress concentration factors at fillets, corners, and holes, but they do not consider the flaws and minute cracks inherent in all materials. When ductile materials such as aluminum, copper, and most steels are stressed, they deform plastically around the tips of these cracks and absorb local overloads. However, when a material cannot behave in a ductile manner, such as when it is near or below its nil-ductility transition temperature, when the strain rate is high (as in impact), or when owing to the effects of high temperature and irradiation the steel becomes relatively brittle, it can fail at a relatively low stress level. This phenomenon should be analyzed using fracture mechanics methods.

The concept of fracture mechanics recognizes the basic phenomena of noncontinuity and nonhomogeneity and provides a numerical method to account for minute cracks in materials. The fracture mechanics design parameters are a toughness (energy absorption) factor, applied stress, size of crack, operating temperature and fluence, and state of stress, which is often far more complex than the state of stress usually assumed.

The major contribution of fracture mechanics is the establishment of the stress intensity factor as the best description of the stress field near a crack tip and the inevitable starting point of any fracture. This factor is a function of part geometry, state of stress in the part, applied load, and size, location, and orientation of the hypothetical crack.

The potential for brittle fracture is considered and fracture mechanics analysis is required if, for (1) a defined minimum flaw size a_m, (2) a critical stress intensity factor K_i, and (3) a shape factor Q, the critical stress for unstable crack propagation σ_k, as defined by (Ref. 26),

$$\sigma_k = \frac{K_i}{Q\sqrt{\pi a_m}} \quad , \tag{1}$$

is less than the minimum yield stress σ_y at temperature for the irradiated material or is 2.7 times the minimum yield stress σ_y at temperature for the unirradiated material.

It has been shown that the locally elevated stress fields around a crack are related to a stress intensity factor. Brittle fracture occurs when the stress intensity factor reaches a critical value; this value can be experimentally determined. The following procedure is recommended for analysis of flaw-sensitive materials according to Ref. 26:

1. On an elastic basis, ascertain the critical stress areas in the component. These areas are determined by reviewing (a) the gross elastic stress distribution throughout the structure and (b) the local environment. The gross elastic stress distribution is defined as the stress calculated, without the presence of a crack, from classical analytic models or finite element techniques.

2. From Ref. 23, determine the minimum value of K_i (K_c, K_{1c}, or applicable value) for the material in specific operating environments. Where data are not available in Ref. 23, the designer is required to furnish experimental data or correlations.

3. Determine the flaw types and sizes in the critical stress areas. If no identifiable flaws are present, a conservative crack size is assumed to exist in the worst location and be oriented in the worst direction. This assumed flaw size shall be at least as large as the minimum size flaw which is readily detectable by standard inspection techniques and shall include crack growth during operation.

4. Select a fracture mechanics model which approximates as closely as possible the stress geometry situation being investigated.

5. Compare the characteristic stress associated with the fracture mechanics model with the allowable stress intensity limit. The

characteristic stress is determined from the gross elastic stress distribution as follows: a stress comparison is made, and the characteristic stress as determined above must not exceed the allowable stress limit; i.e.,

$$\bar{\sigma} \leq 0.6\sigma_K' \quad ,$$

where σ_K' is the critical stress intensity for the geometry being analyzed.

REFERENCES

1. Malek, G. J., "Development of the Flow Analysis Code FLAC," USAEC Report GA-9482, General Dynamics, General Atomic Division, June 1969.
2. Marksberry, C. L., "FLAC73, 1973 Status of FLAC, A Flow Network Analysis Code," General Atomic Report GA-D12942, March 1974.
3. Welty, D. H., "SPIFFS User's Manual," Shell Oil Report P1380038, August 1973.
4. Chiger, H. D., and B. E. Boyack, "Verification of the SPIFFS Computer Program," General Atomic Report GA-A13074, July 1974.
5. Idel'chik, I. E., Handbook of Hydraulic Resistance. Coefficients of Local Resistance and of Friction, U.S. Atomic Energy Commission, 1966 (AEC-tr-6630).
6. Goodman, J., et al., "The Thermodynamic and Transport Properties of Helium," General Atomic Report GA-A13400, October 1975.
7. Delmarva Power and Light Company, "Summit Power Station Preliminary Safety Analysis Report," 1973 (AEC Dockets 50-450, 50-451), question 3.9-1.
8. Boonstra, R. H., "TAC2D - A General Purpose Two-Dimensional Heat Transfer Computer Code. User's Manual," General Atomic Report GA-A14032, July 15, 1976.
9. Morcos, S. M., and K. A. Williams, "The TAC2D Code, Version TFMABC 75-1, Part C: Code Verification and Benchmark Problems," General Atomic Report GA-A13415, June 1975.
10. Smith, J. P., "SINDA User's Manual," TRW Systems Group Reprint 14690-H001-RO-00, Rev. 1, October 1972.
11. "300-MW(e) Gas-Cooled Fast Breeder Reactor Demonstration Plant," General Atomic Report GA-A13045, July 15, 1974.

12. "Gas-Cooled Fast Breeder Reactor Quarterly Progress Report for the Period May 1, 1975 Through July 31, 1975," ERDA Report GA-A13565, General Atomic, October 2, 1975.
13. "Gas-Cooled Fast Breeder Reactor Quarterly Progress Report for the Period February 1, 1975 Through April 30, 1975," ERDA Report GA-A13458, General Atomic, July 17, 1975.
14. "Gas-Cooled Fast Breeder Reactor Quarterly Progress Report for the Period August 1, 1974 Through October 31, 1974," USAEC Report GA-A13238, General Atomic, December 12, 1974.
15. "Gas-Cooled Fast Breeder Reactor Quarterly Progress Report for the Period November 1, 1975 Through January 31, 1976," ERDA Report GA-A13815, General Atomic, March 22, 1976.
16. Soo, P., "Analysis of Structural Materials for LMFBR Coolant - Boundary Components Materials Property Evaluations," USAEC Report WARD-3045T3-5, Westinghouse Electric, November 1972.
17. Simnad, M., "Evaluation of Materials for the GCFR Radial, Upper, and Lower Shield," General Atomic, to be published.
18. Wrights, G. N., "Clinch River Breeder Reactor (CRBR) Shielding Considerations to Assure Structural Integrity," Trans. Am. Nucl. Soc. 22, 788-789 (1975).
19. "Clinch River Breeder Reactor Project Preliminary Safety Analysis Report," Project Management Corporation (NRC Docket 50-537).
20. Nuclear Systems Materials Handbook, v. 1, book 1, Hanford Engineering Development Laboratory (TID-26666).
21. "ASME Boiler and Pressure Vessel Code, 1974 Code Cases," July 1, 1974, Case 1592-4.
22. Odquvist, F. K., Mathematical Theory of Creep and Creep Rupture, Oxford at the Clarendon Press, Oxford, 1966.
23. Hult, J. A., Creep in Engineering Structures, Blaisdell, Waltham, Massachussets, 1966.
24. Penny, R. K., and D. L. Marriott, Design for Creep, McGraw-Hill, New York, 1971.
25. Manson, S. S., Thermal Stress and Low-Cycle Fatigue, McGraw-Hill, New York, 1966.

26. McAfee, W. I., and T. W. Pickel, "Preliminary Elevated-Temperature Core Structures Design," Oak Ridge National Laboratory Report ORNL-TM-4932, 1976.

27. Osgood, C. C., "A Basic Course in Fracture Mechanics," Mach. Des. 58-160 (1971).

28. Tetelman, A. S., and A. I. McEvily, Jr., Fracture of Structural Materials, John Wiley and Sons, New York, 1966.

29. Baroch, C. I., Properties of Reactor Structural Alloys After Neutron or Particle Irradiation, ASTM Special Technical Publication 570, 1975.